Geotech Geol Eng (2022) 40:677–696
https://doi.org/10.1007/s10706-021-01915-8

ORIGINAL PAPER

A Feasibility Study on The Implementation of Neural Network Classifiers for Open Stope Design

Amoussou Coffi Adoko · Festus Saadaari · Daniel Mireku-Gyimah · Askar Imashev

Received: 19 November 2020 / Accepted: 21 June 2021 / Published online: 6 July 2021

Abstract Assessing the stability of stopes is essential in open stope mine design as unstable hangingwalls and footwalls lead to sloughing, unplanned stope dilution, and safety concerns compromising the profitability of the mine. Over the past few decades, numerous empirical tools have been developed to dimension open stope in connection with its stability, using the stability graph method. However, one of the principal limitations of the stability graph method is to objectively determine the boundary of the stability zones, and gain a clear probabilistic interpretation of the graph. To overcome this issue, this paper aims to explore the feasibility of artificial neural network (ANN) based classifiers for the design of open stopes. A stope stability database was compiled and included the stope dimensions, rock mass properties, and the stope stability conditions. The main parameters included the modified stability number (N'), and the stope stability conditions (stable, unstable, and failed), and hydraulic radius (HR). A feed-forward neural network (FFNN) classifier containing two hidden layers (110 neurons each) was employed to identify the stope stability conditions. Overall, the outcome of the analysis showed good agreement with the field data; most stope surfaces were correctly predicted with an average accuracy of 91%. This shows an improvement over using the existing stability graph method. In addition, for a better interpretation of the results, the associated probability of occurrence of stable, unstable, or caved stope was determined and shown in iso-probability contour charts which were compared with the stability graph. The proposed FFNN-based classifier outperformed the conventional stability graph method in terms of accuracy and better prabablistic interpretation. It is suggested that the classifier could be a reliable tool that can complement the conventional stability graph for the design of open stopes.

Keywords Open stope stability · Hydraulic radius · ANN classifiers · Stability graph · Hangingwall · Footwall

A. C. Adoko (✉)
School of Mining and Geosciences, Nazarbayev University, Nur-Sultan city 010000, Kazakhstan
e-mail: amoussou.adoko@nu.edu.kz

F. Saadaari · D. Mireku-Gyimah
Mining Engineering Department, University of Mines and Technology, Tarkwa, Ghana

A. Imashev
Department of Development of Mineral Deposit, Karaganda Technical University, Karaganda 100027, Kazakhstan

1 Introduction

In open stope mining, the stability of the stopes influence the productivity of the mine as instabilities in the stope walls including blasting overbreak,

sloughing, caving or failure of the hangingwalls may lead to delays in production, a high cost of maintenance, high dilution, destruction to machinery, and compromise the safety of the personnel. One of the charateristics of the open stope mining methods is the high productivity where large stopes are developed with a high level of mechanization. However, stopes of large dimensions can be associated with large volume of overbreak, reducing stability and ultimately leading to poor profitability if the practicable maximum dimensions are overlooked (Pakalnis 2015; Pakalnis et al. 1995). While dimensioning the open stopes, it is necessary to account for influencing factors such as induced stress, rock mass mechanical properties, stope geometries, operational constraints, and geological features. Nevertheless, it may not be always practical to consider each of these factors when designing the stopes. This has obviously contributed to the development of many design tools.

As matter of fact, over the past few decades several tools or methods have been successfully proposed for the design of open stope. These include numerical modelling (Heidarzadeh et al. 2018; Henning and Mitri 2007), analytical methods (Diederichs and Kaiser 1999), back analysis of stope performance data in situ measurements (Cepuritis et al. 2010), and empirical tools (Clark 1998; Mathews et al. 1981; Mawdesley et al. 2001; Sunwoo et al. 2006; Suorineni 2010; Vallejos et al. 2017). Each has their advantages and limitations. For example, the analycal methods which rely on the classical analysis of instability around excavtions based on stress criteria for stress driven failure and on limit equilibrium analysis for structurally controlled failure, cannot be always realistic due to the different assumptions involved in these analyses. While numerical modeling is a convenient tool to simulate the mechanical response of the stopes, it may require a lot of modelling effort. This is especially true for realistic simulation of complex conditions since the mechanisms involved in the physical process of open stope mining would necessitate a thorough knowledge of the modelling theory. Besides reliable rock mass properties data that must be used as imputs for the simulation can be difficult to obtain before the stope development. These limitations make the empirical methods more desirable. The stability graph method and its variants appear to be the most commonly used in practice due to their simplicity (Diederichs and Kaiser 1996; Mawdesley et al. 2001; Zhalel et al. 2020).

Nevertheless, a major downside of the stability graph is the subjectivity in the stability's determination zones, which represents a challenge for a less experienced user of the stability graph method. Hence, this inherent subjectivity has resulted in the proposition of several stability graphs with varying stability zones. This variety is due to the fact that the rock mass sloughing and instabilities around mine stope involve several factors that unfortunately can not all be considered in the stability graph method, which was originally introduced as a non-rigourous but handy method (Stewart and Forsyth 1995). Hence, to reduce the subjectivity associated with the determination of the design zones of the graph, it seems very appropriate to interprete the graph in terms of probability. Diederichs and Kaiser (1996) through probabilitic simulation with the consideration of the variability of the imputs of the stability graph, indentified the isoprobability contours of the design limits to account for the uncertainties inherent in the design process. This enabled them to determine the probabilities of stability, failure, and major failure for a given design. Since then, there have been various attempts to remove or at least reduce the subjectivity in the delineation of the zones by generating isoprobability contours using logistic regression techniques (Capes 2009; Mawdesley et al. 2001; Zhalel et al. 2020) and as well as through Bayesian discriminant analysis (Suorineni et al. 2001).

Similarly, the objective of this study is to explore the feasibility of using artificial neural network (ANN) classifiers for the design of open stopes. This is justified by the need for a continual improvement and optimization of the use of the empirical stability graph method in the mining industry. Stope performance data have become increasily available and ANN is a useful tool to that can enable to evaluate the stope walls geo-mechanical responses on the basis of available data. The literature reveals a number of recent applications of artificial intelligence techniques related to stope design and underground excavation excavations. These include for instance, the design of underground excavation spans using artificial neural network (Wang et al. 2002); hard-rock stope span design in entry-type excavations using learning classifiers (García-Gonzalo et al. 2016); open stope stability analysis using the random forest algorithm

(Qi et al. 2018a); prediction of stope stability based on several machine learning algorithms (Qi et al. 2018b, 2018c); open stope stability assessment through artificial intelligence (Santos et al. 2020); and mine stope performance assessment through classifers (Adoko et al. 2019). While in these studies, the focus was mainly on the development of models capable of achieveing a high prediction capability, very limited effort was dedicated to the practical implementation of the ANN for open stope design. Thereofore, in this paper ANN classifiers are used to bridge the existing gaps, and new stability charts will be developed on the basis of the network output, without any hard stability delineation (as commonly used in the conventional stability graph method).

2 Brief Review of the Stability Graph Method

Introduced by Mathews et al. (1981), the stability graph method uses the concept of a stope stability number (N) which incorporates rockmass quality and induced stress, to evaluate the critical dimensions of the stope. This is expressed in terms of the hydraulic radii (HR) of the roof and walls, that ensure stability of the stope. Since the establishment of the original stability graph, several contributions including the modification of the adjustment factors of the stability number, expanding the stability database and extending the stability graph to other mining methods, were made in form of either a qualitative or quatitative stability graph with the purpose of improving the method and reducing the subjectivity in the determination of the stability zones (Capes 2009; Clark 1998; Mathews et al. 1981; Mawdesley et al. 2001; Stewart and Trueman 2004; Stewart and Forsyth 1995; Vallejos et al. 2016). As a result, the literature counts today many versions of stability graphs. Among these, the original stability graph (Mathews et al. 1981) and the modified stability graph (Potvin 1988) are the most widely adopted graphs for a qualitative assessement of stope stability, while the Equivalent linear overbreak or slough (ELOS) stability graph is used to quantify dilution in stopes, hence the quantitative stability graph (Clark and Pakalnis, 1997). However, the ELOS graph was devised to apply to narrow vein deposits and relatively smaller stopes (Clark 1998).

In the stability graph method two main parameters have to be calculated: the stability number N and the hydraulic radius HR. The stability number N is defined in Eq. 1 as:

$$N = Q' \times A \times B \times C \tag{1}$$

where A is the rock stress factor, B is the joint orientation adjustment factor, and C is the gravity adjustment. These factors are determined using Fig. 2. Q' characterizes the rock mass quality and defined in Eq. 2 as:

$$Q' = \frac{RQD}{J_n} \times \frac{J_r}{J_a} \tag{2}$$

where RQD is rock quality designation, J_n is joint set number, J_r is joint roughness number, and J_a is joint alteration number.

Hydraulic radius (HR) refers to the ratio of the stope face area to the stope face perimeter as shown in Eq. 3:

$$HR = \frac{\text{Area } (m^2)}{\text{Perimeter } (m)} \tag{3}$$

Some of the versions of stability graphs are shown in Fig. 1a–c. The use of these chart is quite simple. A new stope data point given by its N value is superimposed on the chart to determine the corresonding HR value of stope surface (roof or walls) that falls within the stability zone (i.e. ensuring stability) (Fig. 1a–c).

3 Methods

3.1 Neural Network Based Classifiers

Artificial neural networks (ANNs) are simulation tools that can detect complex relations such as patterns, correlation, or clusters that exist in a sample data. They do this by mimicking cognitive processes of the human brain through several layers of input and output sample data. The ANN is comprised of compactly interconnected neurons that forms the basic processing units of the network. Hence, hefty analogous computations are executed by the neurons. ANNs can be grouped as feed-forward, back-propagation, dynamic, and counter-propagation networks depending on the training algorithm. A neuron accepts an n input data, and processes the data to present a single output expressed in Eq. 4 as:

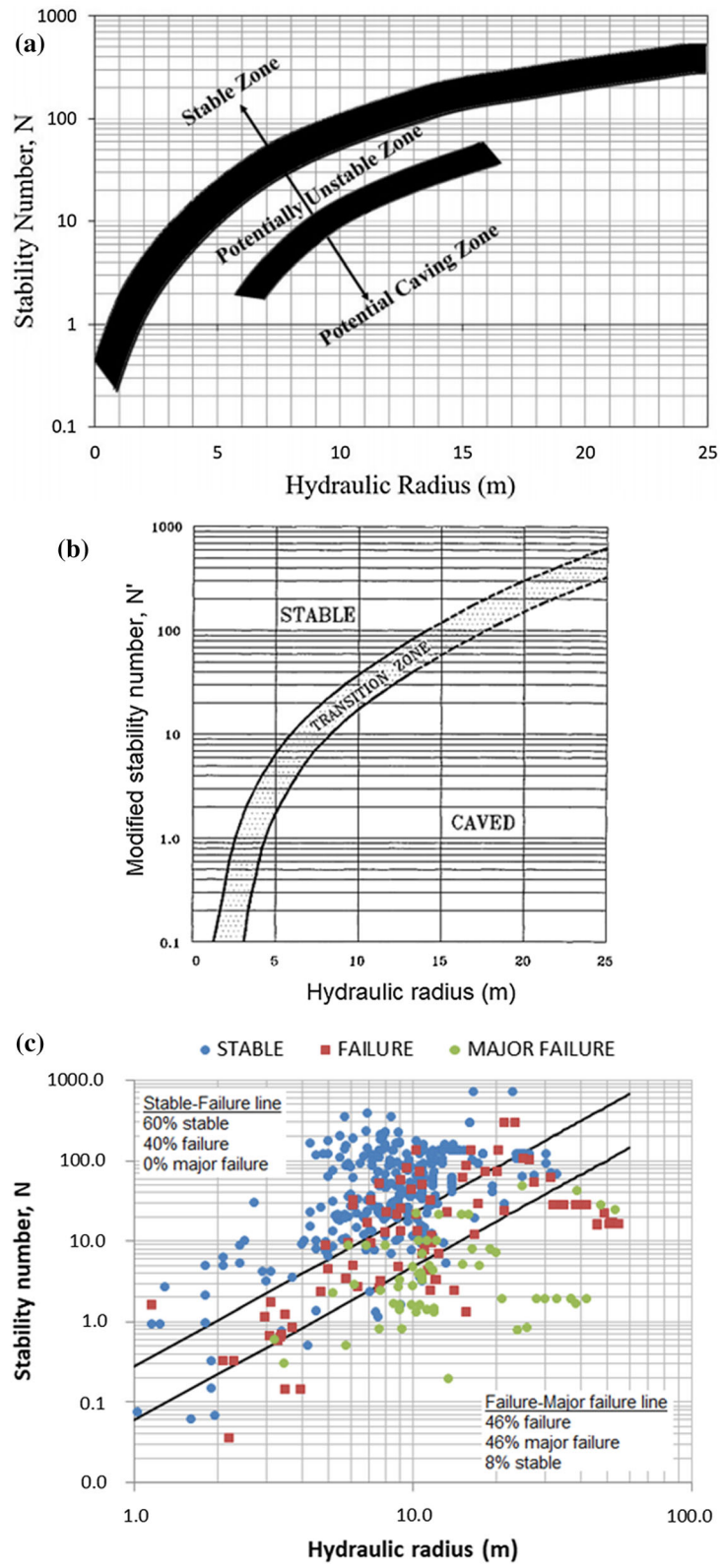

Fig.1 **a** The original stability graph (Mathews et al. 1981) **b** Modified stability graph (Potvin 1988) **c** Extended stability graph after Mawdesley et al. (2001)

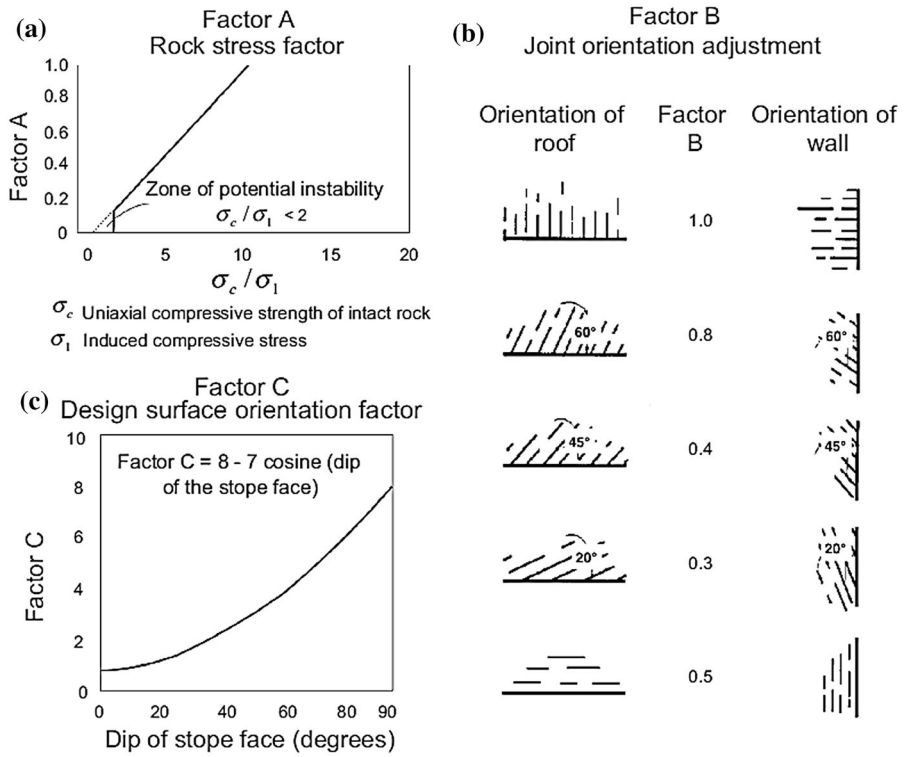

Fig. 2 Adjustment factors of the stability graph after Mathews et al. (1981)

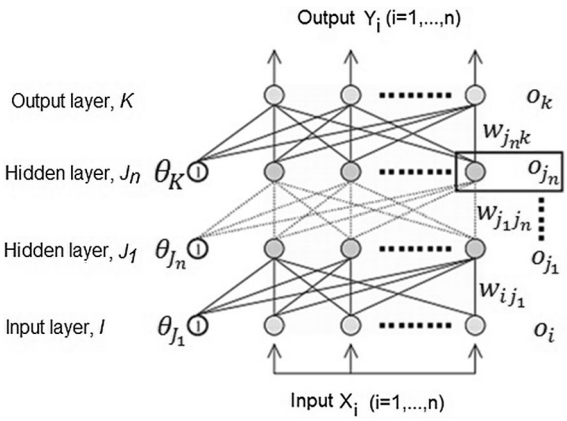

Fig. 3 FFNN schematic diagram

$$y = f\left(\sum_{i=1}^{n} w_i x_i + \theta\right) \tag{4}$$

where f,w_i,x_i and θ represents the values of the activation function of the neuron, the ith weight, the ith input and the bias of the neuron respectively. Equation 4 is simply rewritten as seen in Eq. 5

$$\mathbf{y} = \mathbf{f}(\mathbf{wx} + \mathbf{b}) \tag{5}$$

where the input vector is $\mathbf{x}$ which takes the form $n \times 1$;is bias vector and is the output vector with both being1×1; the weight matrix w is$1 \times n$ and the activation function represented by $\mathbf{f}$, is a1×1 vector.

Each of the network layers has a particular function as either an input layer, hidden layers, and output layer. A layer possesses at least two neurons. There are several kinds of network which are commonly classified based on the network configuration. The feed-forward neural network (FFNN), is a type of ANN which does not require feedback element. An illustration of a typical FFNN structure is provided in Fig. 3. The inputs are established and transmitted forward through all the subsequent layers to obtain the ultimate outputs. The FFNN can equitably approximate any function as recommended by the literature (Engelbrecht 2007). During the beginning of the network training process, initial values of the weights and biases are randomnly assigned. Later, these biases and weights are further attuned to comparing the target and output values until a point where the network outputs

correspond to the targets. The quick performance indicator commonly used here, is the sum of squared errors. Meanwhile to minimize the errors, the Levenberg–Marquardt algorithm is used (Engelbrecht 2007). However, ANNs have been criticized for not performing well when there is a need for extrapolation or when the range surpasses that of the database employed in the calibration of the network. In addition, the training data experiences over-fitting, where the training dataset has been memorized by the network, and hence, the network fails to properly generalize the learned relationship between input and target (Demuth and Beale 2002).

According to Engelbrecht (2007), the feed-forward network (FFNN) can be used as a classifier and can be also employed to fit data as it can fairly estimate any kind of function.

Depending on the feature of the patterns to be recognized in a classification task, the structures to be used are countless (Lam et al. 2014). The basic principle of these classifiers is their input pattern which is presented as $\mathbf{x}(k) = \{x_1(k), x_2(k), ..., x_n(k)\}$ and is the featured vector of an object of interest being identified. This allows the feature patterns to be grouped into classes of N through a supervised learning. As an illustration of the principle, for example, in the one-against-all classifier, which is characterized by a multiple-input–single-output, FFNN which is fully connected the $\mathbf{x}$(k) is then processed as input and correlated to the target to generate a single value $\mathbf{y}(k) = \{y_1(k), y_2(k), ..., y_n(k)\}$ as output. The target output $\mathbf{y}^d(k) = \{y_1^d(k), y_2^d(k), ..., y_n^d(k)\}$ $y^d(k)$ takes value of $C_i = \{c_{i1}, c_{i2}, ..., c_{in}\}, i = 1, ...N$. Each time the input feature pattern $\mathbf{x}$(k) corresponds to the class i. A training algorithm allows the output $\mathbf{y}(k)$ to be in the maximum proximity to $\mathbf{y}^d(k)$ under the class, where $\mathbf{x}$(k) corresponds to. The output class j is being represented by:

$$j = \arg\min_i \{|\mathbf{y}(k) - C_i|, i \in \{1, ...N\}\} \quad (6)$$

where |.| refers to the Euclidean norm. In case the set j comprises over one element, then the element emerging first in the set is then recognized as the class label.

3.2 Data Source and Data Description

A total of 225 stope case histories were recorded over three months across three different underground mines in Ghana, West Africa. Of the 225 case histories, 132 of them were obtained from Paboase underground mine of Kinross Chirano Gold Mine Limited, and 76 cases were recorded from B, an undisclosed mine because of confidentiality agreement undertaken covering the case histories. Hence the company's identity is represented by B, while the remaining 17 cases were obtained from AngloGold Ashanti, Obuasi.

The orebody from AngloGold Ashanti mine, Obuasi comprises mainly sulphides and some percentage of quartz material. It is characterized by cross joints forming rock blocks at the back of the excavation. Foliation planes are present and they are parallel to the walls of the excavation. The ground condition is good. The average width of the the orebody in the study range between 4 and 21 m with the dip ranging from 60 to 87°. The rock mass quality of the main rock units is generally fairly good with Q' in the range of 0.97–71. The rock mass of Paboase and Mine B comprise of strong tonalite, quartz dolerite, and dolerite (footwall, orebody, and hanging wall rock masses), and are classed as good to very good rock mass quality with similar rock mass properties. Because of silicification of the rockmass, the orebody has high intact rock strength. The footwall and hanging wall intact rock strength is slightly lower than that of the orebody due to the influence of shears next to the orebody contact. All domains contain two major joint sets plus several minor random joint sets which are moderate to widely spaced joints.

The stope data were obtained from the block and stope notes and other geotechnical reports of the respective companies. The actual hydraulic radii of the stopes were verified using the cavity monitoring system data and mine planning and design files, while the stability number corresponding to each stope surface (N') was determined using the geotechnical database of the various mines which included the stope performance. Meanwhile the adjustment factors to calculate N' were determined per Sect. 2.1. A thorough review of the geotechnical databases was undertaken to eliminate outliers and to recover some missing data. The 225 stope surface cases were grouped as stable (102 cases), unstable (85 cases), and caved (38 cases) representing 45%, 38% and 17%

of the database, respectively. A data sample and a statistical description of the employed dataset are given in Table 1 and Table 2, respectively. Meanwhile, the whole data is provided in Appendix 1 (supplementary material).

4 Results

4.1 Model Configuration

The stope stability dataset (225 cases) that have been compiled for the research was randomly split into three datasets; the training, validation, and testing datasets consisting of 70%, 15%, and 15% of the data, respectively, as commonly suggested (Demuth and Beale 2002; Rafiai and Moosavi 2012). The vectors (1,0,0), (0,1,0) and (0,0,1) were assigned to the dependent parameters to be classified (i.e. stope surface stability condtions): stable (Class 1), unstable (Class 2), and caved (Class 3), respectively. The computations were done using the the MATLAB software (Neural Network toolbox). To arrive at a decisive result, there was the need to identify the optimal network architecture. Hence, an iterative series of trials were performed using 1 to 3 hidden layers while varying the number of neurons to a maximum of 200 in each case. Logsig in Eq. (7) and softmax in Eq. (8) transfer functions were applied to the the hidden and output layers, respectively.

Table 2 Statistical description of the dataset

Parameters	HR	Q'	N'	Stope condition
Unit	m	%	–	Logic
Max	19.22	71.25	570.00	Stable
Min	1.90	0.10	0.40	Caved
Mean	6.66	11.63	28.07	–
St. dev	2.88	14.56	68.52	–

$$\log sig(n) = \frac{1}{1 + e^{-n}} \tag{7}$$

$$soft\max(n) = \frac{e^{n}}{\sum e^{n}} \tag{8}$$

The performance of the networks was evaluated using the cross-entropy algorithm as illustrated in (Fig. 4), with the best validation performance during the experiments being 0.14 at epoch 76. A summary of some of the trials is provided in Table 3 where the network sizes, the validation errors, and the confusion values are shown. It can be seen that the 2-hidden layer FFNN (highlighted in bold) with 110 neurons in each layer was the most appropriate. However, the network with one hidden layer (also highlighted in bold) containing 36 neurons yielded lowest validation error; but inspection of the training error showed quite large value which means the network has not been properly trained. Hence this network was not selected as the optimum of the experiments.

Table 1 Data sample

Stope surfaces	Orebody width (m)	HR (m)	Q'	A	B	C	N'	Stope condition
Back	10.7	3.73	4.70	1.00	1.00	1.00	4.70	Unstable
Hanging Wall	12.00	7.89	3.81	0.60	0.28	7.06	4.52	Caved
Hanging Wall	6.40	8.84	1.50	1.00	0.50	8.00	6.00	Caved
Foot Wall	6.40	8.84	4.70	1.00	0.80	8.00	30.08	Unstable
Back	5.24	2.30	4.70	1.00	1.00	1.00	4.70	Stable
Vertical End	5.24	2.23	4.70	1.00	1.00	8.00	37.60	Stable
Hanging Wall	5.24	8.38	0.20	1.00	0.50	8.00	0.80	Caved
Foot Wall	5.24	8.38	4.70	1.00	0.80	8.00	30.08	Unstable
Back	6.00	2.80	4.70	1.00	1.00	1.00	4.70	Stable
Vertical End	6.00	2.50	4.70	1.00	1.00	8.00	37.60	Stable

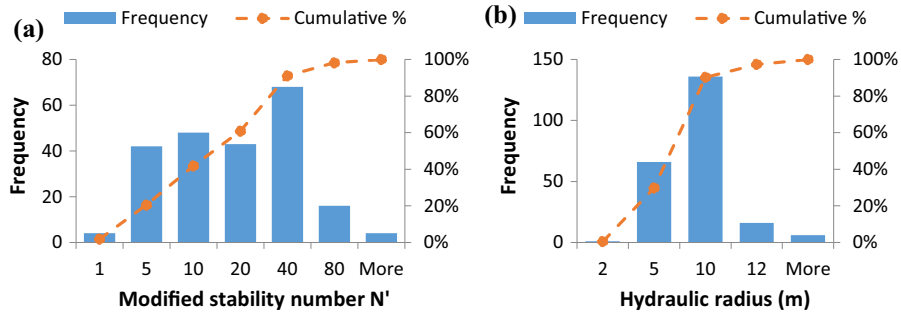

Fig. 4 **a** Distribution of the modified stability number N'. **b** Distribution of the hydraulic radius

Table 3 Summary of the FFNN experiments

Neuron number in hidden layer	Validation error	Confusion value	Neuron number in hidden layers	Validation error	Confusion value
8	0.39	0.27	10–10	0.29	0.17
10	0.26	0.16	20–20	0.20	0.10
12	0.21	0.14	30–30	0.19	0.12
14	0.38	0.30	60–60	0.29	0.34
16	0.46	0.32	80–80	0.28	0.17
18	0.18	0.14	100–100	0.21	0.13
20	0.29	0.31	**110–110**	**0.14**	**0.09**
30	0.49	0.29	112–112	0.24	0.46
36	**0.12**	**0.11**	120–120	0.23	0.14
50	0.38	0.20	160–160	0.35	0.20
60	0.20	0.16	200–200	0.26	0.20
70	0.36	0.26	10–10–10	0.14	0.13
80	0.31	0.16	20–20–20	0.34	0.16
90	0.39	0.19	100–100–100	0.31	0.13
100	0.30	0.16	160–160–160	0.32	0.21
110	0.31	0.20	180–180–180	0.25	0.14
150	0.28	0.14	190–190–190	0.17	0.11
200	0.70	0.23	200–200–200	0.20	0.12

4.2 Classification Results and Classification Evaluation

The confusion matrix of the model was obtained and the results of the classifications are summarized in Tables 4, 5. In Table 4. It can be seen that 96 cases of stable stopes were properly classified; 6 cases were misclassified as unstable; no cases were classified as caved. The overall percentage of correct classification is 90.7% which corresponds to a confusion (misclassification) of 9.3%. This value indicates the fraction of samples misclassified during the modelling. It was found that for the training, the validation, and the testing, the specifc confusion values were 8.9%, 8.8% and 11.8% respectively. The overall confusion value was 9.3%. These values are relatively low in comparison with some existing results (see section). This means if 100 new cases of stope surface conditions were to be presented to the FFNN-classifer, 10 cases would likely be misclassified. No stable cases will be misclassified as caved (and vice versa) which is very useful. Hence, the FFNN-classifier yielded high classification accuracy in recognizing the stope wall stability conditions. Nevertheless, it should be noted

Table 4 Overall classification results

Observed	Predicted			Percent Correct
	Stable	Unstable	Caved	
Stable	96	6	0	94.1
Unstable	6	76	3	86.4
Caved	0	6	32	91.4
Overall percentage per class	94.1%	89.4%	84.2%	90.7

that cross validation was not performed on the validation data since the data were already randomly split into training, testing, and validation datasets. This procedure is commonly used when cross validation is not implemented (Adoko et al. 2020).

The classification performance of the FFNN classification is evaluated using the classification indices such as the accuracy, sensitivity (true positive rate), and specificity (false positive rate) as they represent an indicator of the quality of the classification. These can be calculated using Eqs.9–11 where, F_p, T_p,F_n T_n, and stand for: false positive, true positive, false negative, and true negative, respectively.

$$\text{Accuracy} = \frac{T_p + T_n}{T_p + T_n + F_p + F_n} \tag{9}$$

$$\text{Sensitivity} = \frac{T_p}{T_p + F_n} \tag{10}$$

$$\text{Specificity} = \frac{T_n}{T_n + F_p} \tag{11}$$

Table 6 provides a summary of the performance of the FFNN-classifier. It shows that the average accuracy of the classification (as defined in Eq. 9) is 93.78%. The sensitivity of caved cases of stope condition is 84.21%, being the lowest sensitivity values (true positive rate). This also indicates that caved cases are likely to be more misclassified than other cases (Fig. 5).

Table 5 Positive and Negative counts

	Fn	Fp	Tp	Tn
Stable	6	6	96	117
Unstable	9	12	76	128
Caved	6	3	32	184

The receiver operating characteristic (ROC) curve (another indicator of the quality of classifiers) of the classification is plotted in Fig. 6. The ROC uses a specific value of the outputs (threshold) to identify the class to be recognized (i.e. stable, unstable or caved stope walls). Two quantities are evaluated in the curves: false positive rates and true positive rates. When the ROC curves are located on the top left corner and further from the diagonal, the better the performance of the classification. Conversely, when the curve gets closer to the diagonal, a low classification performance is observed. The results comfirm that a very good classification was obtained as the three curves are located on the top left corner. Moreover, the curve corresponding to stable stope (class 1 in blue) is above the other two, which indicates that stable stope surfaces have better performance (highest true positive and lowest false positive rates). Meanwhile, unstable stope surfaces (class 2) have the lowest true positive rate and caved stope surfaces (class 3) have the highest false positive rate. This is in unison with the classification performance from Table 6.

4.3 Comparison of the Ffnn Outputs with the Stability Graphs

The output vectors of the proposed FFNN are employed to plot probability contours and compared to the conventional stability graphs. A sample of the outputs is provided in Table 7. As seen, the first raw of Table 7 shows an output vector [0.0, 0.59, 0.41]; this corresponds to a correct prediction of the target vector [0, 1, 0] which represents unstable stope walls. Next, thin-plate spline interpolant were used to fit the maximum component of the output vectors in Matlab, and excellent fitting accuracy was obtained (with sum of square errors almost zero and R^2 equal to 1).

The contours of the output values are provided in Figs.7a–c. The color code indicates the probability of

Table 6 Classification performance

Performance	Acurracy (%)	Sensitivity (%)	Specificity (%)
Stable	94.67	94.12	95.12
Unstable	90.67	89.41	91.43
Caved	96.00	84.21	98.40
Average	93.78	89.25	94.98

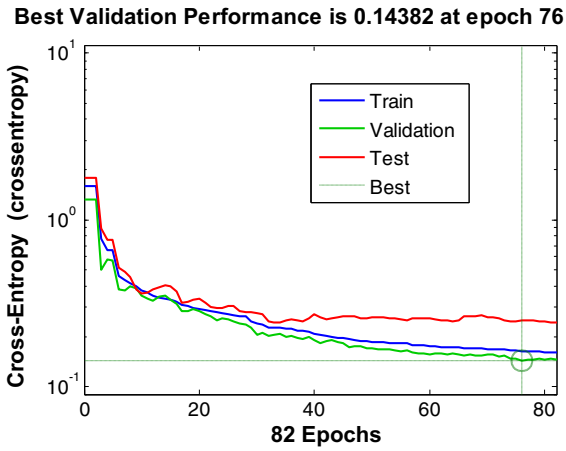

Fig. 5 Network performance (errors)

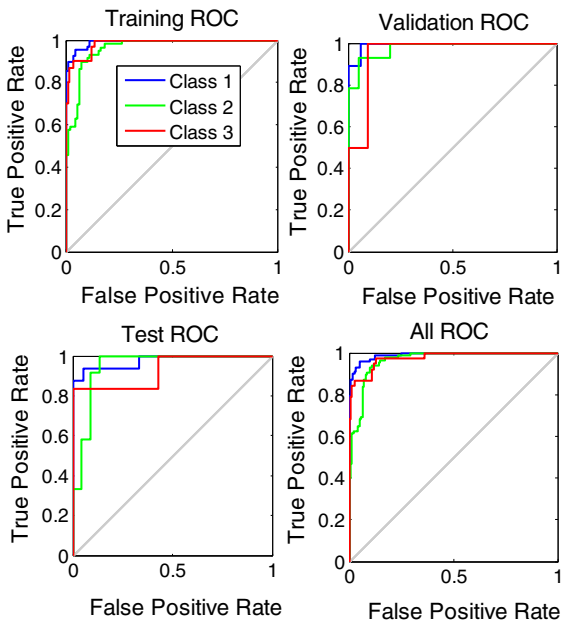

Fig. 6 ROC graphs

the occurrence of the stope surface conditions. Basically, the transfer function *softmax* (see Eq. (8) that has been used in the modelling, returns values in a range of [0,1] representing the probabilities range of the output for obtaining each class of stopes which is very useful.

Figure 7a shows the isoprobability contours for stable stope walls. It can be seen that a probability of

Table 7 Sample of the input, target, and output data of the FFNN

Inputs		Targets				Output vetors		
HR(m)	N'	Actual	Vectors					
7.37	6.70	Unstable	0	1	0	**0.00**	**0.59**	**0.41**
10.26	6.00	Unstable	0	1	0	0.19	0.57	0.24
7.16	4.11	Caved	0	0	1	0.00	0.28	0.72
2.71	37.60	Stable	1	0	0	1.00	0.00	0.00
7.27	6.30	Caved	0	0	1	0.00	0.56	0.44
4.20	13.44	Stable	1	0	0	0.96	0.04	0.00
5.89	15.77	Stable	1	0	0	0.86	0.14	0.00
9.08	30.08	Unstable	0	1	0	0.12	0.88	0.00
9.38	0.40	Caved	0	0	1	0.00	0.03	0.97
7.50	30.08	Stable	1	0	0	0.88	0.12	0.00
8.49	11.42	Unstable	0	1	0	0.00	0.55	0.44
8.84	30.08	Unstable	0	1	0	0.08	0.92	0.00
8.49	4.67	Caved	0	0	1	0.00	0.02	0.98
10.65	30.08	Stable	1	0	0	0.17	0.83	0.00
7.32	25.93	Stable	1	0	0	0.85	0.15	0.00
7.99	1.92	Caved	0	0	1	0.00	0.01	0.99
3.18	37.60	Stable	1	0	0	1.00	0.00	0.00
5.00	13.20	Stable	1	0	0	0.97	0.03	0.00
9.08	10.80	Unstable	0	1	0	0.04	0.59	0.37
10.38	52.00	Stable	1	0	0	0.09	0.91	0.00
6.56	21.60	Stable	1	0	0	0.94	0.06	0.00
4.34	66.40	Stable	1	0	0	1.00	0.00	0.00
4.29	37.60	Stable	1	0	0	1.00	0.00	0.00
3.61	4.70	Stable	1	0	0	0.73	0.27	0.00
7.50	9.84	Unstable	0	1	0	0.00	0.91	0.09
7.37	3.52	Caved	0	0	1	0.00	0.18	0.82
5.56	35.34	Stable	1	0	0	1.00	0.00	0.00
6.00	6.00	Unstable	0	1	0	0.01	0.97	0.01
3.49	37.60	Stable	1	0	0	1.00	0.00	0.00

more than 0.5 (blue, green, and yellow areas) that would correspond to stable stope walls are displayed in the blue, green, and yellow areas. Stope walls with N' = 500 are likely to be stable regardless of the HR values; the same could be said for when N' < 300 and HR < 5 m.

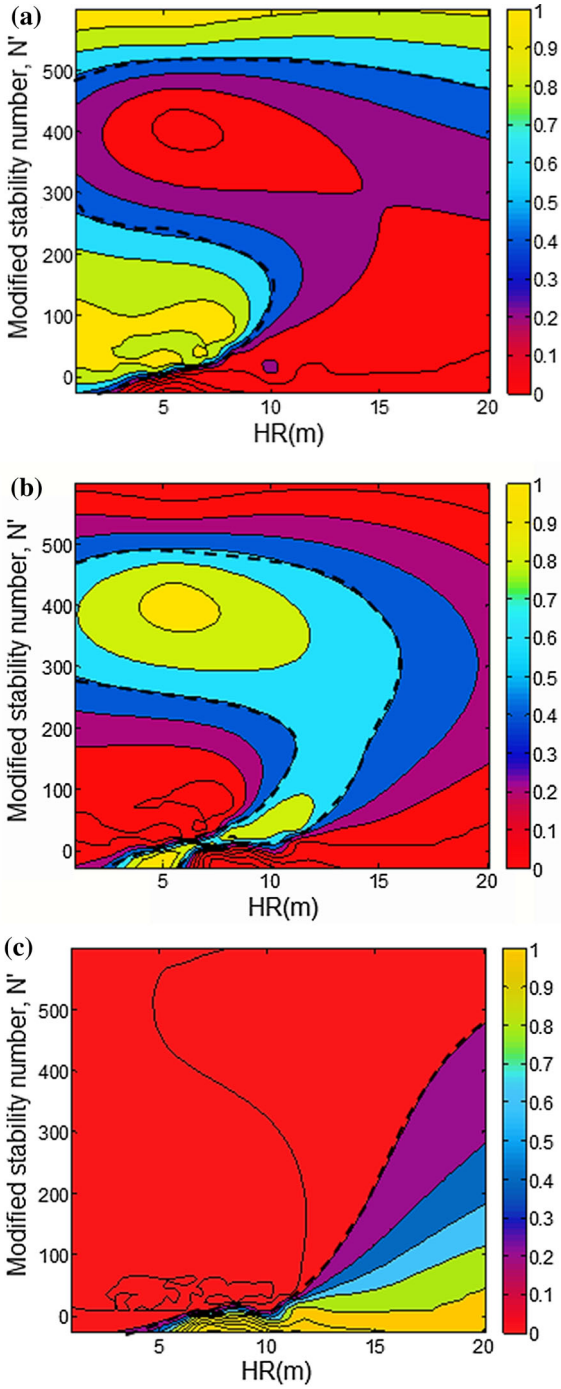

Fig. 7 **a** 2D Isoprobability contour for stable stope walls. **b** 2D Isoprobability contour for unstable stope walls. **c** 2D Isoprobability contour for caved stope walls

In Fig. 8 the stability graph of the data is shown. The stable and the caved boundary lines were determined according to Mawdesley et al. (2001) as $N' = 0.28^{1.9HR}$ and $N' = 0.06^{1.9HR}$, respectively, where logictic regression was used.

Next, a confusion matrix of the graph was established by simply counting the number of data points correctly classified to stope surface conditions as stable (data point above the stable boundary); unstable (data point between the two boundaries); and caved (data point below caved boundary line). The results are summarized in Tables 8, 9.

The misclassification is almost 40% and much lower performance indicators were obtained. This indicates that the proposed FFNN-classifer outperformed the conventional stability graph. This is also true when comparing the results of the present study to those of some previous studies (see Table 10). It should be noted that in Table 10 the confusion values were obtaind based on two categories of the stability conditions (stable and unstable); here unstable include failed and caved surfaces. From Table 4, the new confusion value is has been recalculated as 6%, a bit higher than the previous situation when three categories were considered, which makes sense. Moreover, with the classifer model, there no need for any hard boundary of the stability condition zones. The probabilistic aspect of classifacation becomes compulsory, more intuitive, and straightforward. For example, when a stope wall with N' = 200 is

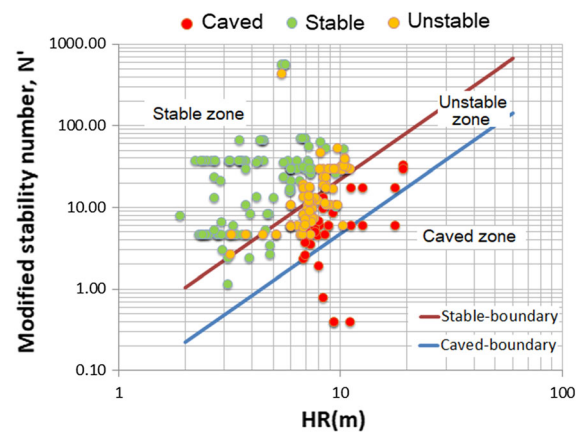

Fig. 8 Stability graph of the data

Table 8 Classification results based on the stability graph

Observed	Predicted			Percent Correct
	Stable	Unstable	Caved	
Stable	96	6	0	94.1%
Unstable	40	45	0	52.9%
Caved	1	30	7	18.4%
Overall percentage per class	70.1%	55.5%	100%	65.77%

Table 9 Classification performance

Performance	Acurracy (%)	Sensitivity (%)	Specificity (%)
Stable	79.11	94.12	66.67
Unstable	66.22	52.94	74.29
Caved	86.22	18.42	100.00
Average	77.19	55.16	80.32

Table 10 Comparison of the FFNN with other studies

Method	Confusion value (%)
Confusion matrix of the conventional stability graph (Potvin 1988; Suorineni et al. 2001)	16–34
Random forest (Qi et al. 2018a)	14–18
Several machine learning algorithms (Qi et al. 2018b)	22–34
Logistic regression (Stewart and Trueman 2004)	10–22
Feedforward Neural Network Classifier (This study)	6

dimensioned in such a way its hydraulic radius (HR) is 10 m, it has about a 50% chance of being stable, a 40% chance of being unstable, and a 10% chance to cave according to the isoprobability contour maps (Figs.7a–c). On the other hand, with the stability graph (Fig. 8), the stope wall will be classifield as stable with an unknown probability of occurrence. These data highlight one of the weaknesses of the conventional stability graph.

5 Discussions

Despite the high accuracy of the classification as revealed by these results, the outputs demonstrate that the FFNN-classifier does not identify caved stope cases very well as 6 out of 38 cases (i.e. 16%) were misclassified as unstable. If new data (assuming that the new dataset is statistically identical), were to be evaluated by the proposed FFNN-classifier, there would likely be 16 out of 100 misclassified unstable cases. This still outperforms the stability graph method (30 out 38 cases of caved stopes were classified as unstable; and 1 was even classified as stable). Nonetheless, the classifier can distinguish very well between the stable and caved cases (zero cases of caved were misclassified as stable cases). Hence, this is the most essential capability of the proposed FFNN-classifier. It is a very useful approach to classifying the stability of stope faces along with a probabilistic interpretation of the network outputs in the form of charts.

The results suggest that the conventional stability graph is not a good predictor of stope surface stability. Usually, in order to enhance the performance of the stability graph, outliers are eliminated from the data. This implies that deep knowledge of the site conditions is important to properly identify outliers. For example, the stope surface corresponding to the datapoint (N' = 437; HR = 5.43 m; unstable) could be an outlier since the instability could be due to some operational constraints (blasting effects) or local geological conditions. Even if this outlier was removed from the database, there will not be significant improvement of the stability graph method. Conversely, when the outlier was removed and the

FFNN output plot showed significant changes, as given in Fig. 9, in short, the FFNN-classifer could be considered as an improved version of the stability graph as they use/share the same imputs.

Some of the limitations linked to this study include the quality, the range, and the size of the data used because this ANN-classifier performance depends heavily on the input data. Imbalance in the dataset results in the model prediction ability to be biased toward the most representative stable class. In this study, 45%, 38%, and 17% of stable, unstable, and caved cases of stope faces respectively. In order to use the proposed model to assess fresh cases of stope stability, it is recommended that new data be of similar proportion for optimal performance. Hence, this could bias the inputs and prediction ability of the FFNN-classifier. Therefore, sound engineering judgment must follow the implementation of this classifier. Another limitation is that the proposed model does not quantify the uncertainty related to the input parameters. So it should not be used for that purpose. In addition, the results of the study imply that the model is highly site-sensitive. In other words, the results will vary depending on the specific site (with specific data range) where the stopes are excavated. However, some reseachers have argured that site-specificity has little effect on the stope surface stability assessment using the stability graph method (Mawdesley et al. 2001). The FFNN model has the capability to accommodate more input parameters. The whole parameters of the database could be used to train the model without necessarily using the concept of stability number and hydraulic radius, and without any limitation of computation capacity thanks to the current availability of faster computers. Further studies could explore that possibility, further enhancing the modeling of stope surface stability conditions in open stope mining.

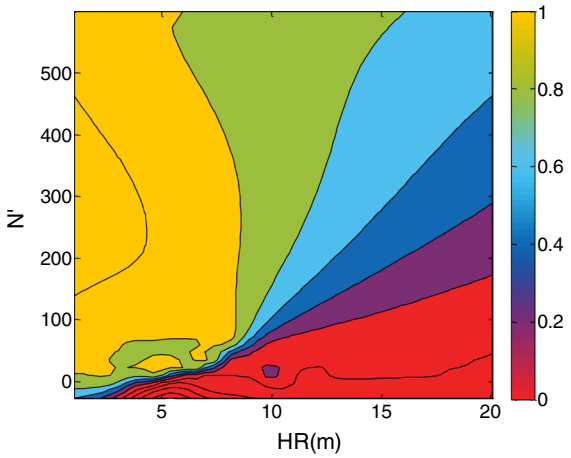

Fig. 9 2D Isoprobability contour for stable stope walls with an outlier removed

Finally, as a suggestion for practical use of this method to evaluate the stability conditions of open stope walls, users no not have develop their own FFNN. The network may be recalibrated to reflect the data range of the specific site. Once a new data point is presented to the network, the network returns the stability condition but also the probability as well. This allows selecting the dimensions of the stope (i.e. HR) that would reduce instabilities such as sloughing. However, for those users who prefer using empirical charts, they can use the porposed chart (Fig. 9) which can be also considered as an enhanced version of the stability graph for open stope design.

6 Conclusion

In this study, a stope wall stability classifier model was proposed. Case histories of underground mine stope surfaces (hangingwall, footwall, and back) stability data were collected. The data included the geometry of the stopes, the rock mass parameters, and stability conditions of stopes (stable, unstable, and caved). A FFNN-classifier having two hidden layers and 110 neurons in each layer is applied to identify each of the the stability classes. The classification results showed an excellent performance of the model. The FFNN-classifier could distinguish each stope surface condition with high accuracy. The overall misclassification was less than 10% while the conventional stability graph methods yielded a misclassication of almost 40%. This indicates improvement over the conventional stability graph method. In addition, probability contour plots were established using the model output. These plots offer a better interpretation of the model results and provide the associated probability of occurrence of stable, unstable, or caved stope surfaces.

It should be noted that the current results are dependent on the range and dimension of the dataset used; therefore generalisation can only be possible for a similar dataset. The current results can help establish more detailed stability charts for tunneling and mining applications. Further studies may look into increasing

the size of the database (and the range of the data), and recalibrating the FFNN-classifier to achieve better accuracy. Also, more parameters known to affect the stope surface conditions could included in the FFNN-model. It is recommended that the FFNN-classifier could serve as a basis for underground excavation design and the mitigation of stope stability problems along with existing empirical charts, and adequate engineering judgment.

Acknowledgements The Faculty Development Competitive Research Grant program of Nazarbayev University, Grant N° 090118FD5338 supported this study. The authors acknowledge the contribution of the authorities of Kinross Chirano Gold Mine and AngloGold Ashanti Obuasi Mine for providing access to their mine and relevant data for this study.

Funding Nazarbayev University, Grant N° 090118FD5338.

Data Availability Appendix 1.

Code Availability Available upon request.

Declarations

Conflicts of interest All the authors declare that they have no conflict of interest.

Appendix 1

See Table 11.

Table 11 Dataset

Mine Portal	Level	Orebody Thickness	Stope Surface	Surface Dip (°)	Height (m)	Span (m)	Length (m)	HR (m)	Q'	A	B	C	N'	Status
PAB	2000	11.9	Back	90	30.0	11.9	20.0	3.7	4.7	1.0	1.0	1.0	4.7	Unstable
PAB	2000	11.9	VerticalEnd	90	30.0	11.9	30.0	4.3	4.7	1.0	1.0	8.0	37.6	Stable
PAB	2000	11.9	HangingWall	90	30.0	20.0	30.0	6.0	1.5	1.0	0.5	8.0	6.0	Unstable
PAB	2000	11.9	FootWall	90	30.0	20.0	30.0	6.0	4.7	1.0	0.8	8.0	30.1	Stable
PAB	2000	22.3	Back	90	30.0	22.3	43.0	7.3	4.7	1.0	1.0	1.0	4.7	Unstable
PAB	2000	22.3	VerticalEnd	90	30.0	22.3	30.0	6.4	4.7	1.0	1.0	8.0	37.6	Stable
PAB	2000	22.3	HangingWall	90	30.0	30.0	43.0	8.8	1.5	1.0	0.5	8.0	6.0	Caved
PAB	2000	22.3	FootWall	90	30.0	30.0	43.0	8.8	4.7	1.0	0.8	8.0	30.1	Unstable
PAB	2000	10.0	Back	90	30.0	10.0	20.0	3.3	4.7	1.0	1.0	1.0	4.7	Stable
PAB	2000	10.0	VerticalEnd	90	30.0	10.0	30.0	3.8	4.7	1.0	1.0	8.0	37.6	Stable
PAB	2000	10.0	HangingWall	90	30.0	20.0	30.0	6.0	1.5	1.0	0.5	8.0	6.0	Unstable
PAB	2000	10.0	FootWall	90	30.0	20.0	30.0	6.0	4.7	1.0	0.8	8.0	30.1	Stable
PAB	2000	27.0	Back	90	30.0	27.0	26.0	6.6	4.7	1.0	1.0	1.0	4.7	Unstable
PAB	2000	27.0	VerticalEnd	90	30.0	27.0	30.0	7.1	4.7	1.0	1.0	8.0	37.6	Stable
PAB	2000	27.0	HangingWall	90	30.0	26.0	30.0	7.0	1.5	1.0	0.5	8.0	6.0	Unstable
PAB	2000	27.0	FootWall	90	30.0	26.0	30.0	7.0	4.7	1.0	0.8	8.0	30.1	Stable
PAB	2000	9.2	Back	90	30.0	9.2	20.0	3.2	4.7	1.0	1.0	1.0	4.7	Stable
PAB	2000	9.2	VerticalEnd	90	30.0	9.2	30.0	3.5	4.7	1.0	1.0	8.0	37.6	Stable
PAB	2000	9.2	HangingWall	90	30.0	20.0	30.0	6.0	1.5	1.0	0.5	8.0	6.0	Unstable
PAB	2000	9.2	FootWall	90	30.0	20.0	30.0	6.0	4.7	1.0	0.8	8.0	30.1	Stable
PAB	2000	6.4	Back	90	30.0	6.4	43.0	2.8	4.7	1.0	1.0	1.0	4.7	Stable
PAB	2000	6.4	VerticalEnd	90	30.0	6.4	30.0	2.6	4.7	1.0	1.0	8.0	37.6	Stable
PAB	2000	6.4	HangingWall	90	30.0	30.0	43.0	8.8	1.5	1.0	0.5	8.0	6.0	Caved

Table 11 continued

Mine Portal	Level	Orebody Thickness	Stope Surface	Surface Dip (°)	Height (m)	Span (m)	Length (m)	HR (m)	Q'	A	B	C	N'	Status
PAB	2000	6.4	FootWall	90	30.0	30.0	43.0	8.8	4.7	1.0	0.8	8.0	30.1	Unstable
PAB	2000	5.2	Back	90	30.0	5.2	38.0	2.3	4.7	1.0	1.0	1.0	4.7	Stable
PAB	2000	5.2	VerticalEnd	90	30.0	5.2	30.0	2.2	4.7	1.0	1.0	8.0	37.6	Stable
PAB	2000	5.2	HangingWall	90	30.0	30.0	38.0	8.4	0.2	1.0	0.5	8.0	0.8	Caved
PAB	2000	5.2	FootWall	90	30.0	30.0	38.0	8.4	4.7	1.0	0.8	8.0	30.1	Unstable
PAB	2000	6.0	Back	90	30.0	6.0	85.0	2.8	4.7	1.0	1.0	1.0	4.7	Stable
PAB	2000	6.0	VerticalEnd	90	30.0	6.0	30.0	2.5	4.7	1.0	1.0	8.0	37.6	Stable
PAB	2000	6.0	HangingWall	90	30.0	30.0	85.0	11.1	0.1	1.0	0.5	8.0	0.4	Caved
PAB	2000	6.0	FootWall	90	30.0	30.0	85.0	11.1	4.7	1.0	0.8	8.0	30.1	Unstable
PAB	2025	6.2	Back	90	30.0	6.2	30.2	2.6	4.7	1.0	1.0	1.0	4.7	Stable
PAB	2025	6.2	VerticalEnd	90	30.0	6.2	22.0	2.4	4.7	1.0	1.0	8.0	37.6	Stable
PAB	2025	6.2	HangingWall	90	30.0	22.0	30.2	6.4	1.5	1.0	0.5	8.0	6.0	Unstable
PAB	2025	6.2	FootWall	90	30.0	22.0	30.2	6.4	4.7	1.0	0.8	8.0	30.1	Stable
PAB	2025	6.6	Back	90	30.0	6.6	20.0	2.5	4.7	1.0	1.0	1.0	4.7	Stable
PAB	2025	6.6	VerticalEnd	90	30.0	6.6	30.0	2.7	4.7	1.0	1.0	8.0	37.6	Stable
PAB	2025	6.6	HangingWall	90	30.0	20.0	30.0	6.0	2.7	1.0	0.5	8.0	10.8	Unstable
PAB	2025	6.6	FootWall	90	30.0	20.0	30.0	6.0	4.7	1.0	0.8	8.0	30.1	Stable
PAB	2025	13.0	Back	90	30.0	13.0	10.0	2.8	4.7	1.0	1.0	1.0	4.7	Stable
PAB	2025	13.0	VerticalEnd	90	30.0	13.0	30.0	4.5	4.7	1.0	1.0	8.0	37.6	Stable
PAB	2025	13.0	HangingWall	90	30.0	10.0	30.0	3.8	2.7	1.0	0.5	8.0	10.8	Stable
PAB	2025	13.0	FootWall	90	30.0	10.0	30.0	3.8	4.7	1.0	0.8	8.0	30.1	Stable
PAB	2025	19.0	Back	90	30.0	19.0	46.0	6.7	4.7	1.0	1.0	1.0	4.7	Unstable
PAB	2025	19.0	VerticalEnd	90	30.0	19.0	30.0	5.8	4.7	1.0	1.0	8.0	37.6	Stable
PAB	2025	19.0	HangingWall	90	30.0	30.0	46.0	9.1	2.7	1.0	0.5	8.0	10.8	Unstable
PAB	2025	19.0	FootWall	90	30.0	30.0	46.0	9.1	4.7	1.0	0.8	8.0	30.1	Unstable
PAB	2025	7.2	Back	90	60.0	7.2	60.0	3.2	4.7	1.0	1.0	1.0	4.7	Stable
PAB	2025	7.2	VerticalEnd	90	60.0	7.2	61.0	3.2	4.7	1.0	1.0	8.0	37.6	Stable
PAB	2025	7.2	HangingWall	90	60.0	61.0	35.0	11.1	1.5	1.0	0.5	8.0	6.0	Caved
PAB	2025	7.2	FootWall	90	60.0	61.0	35.0	11.1	2.7	1.0	0.8	8.0	17.3	Caved
PAB	2025	8.1	Back	90	60.0	8.1	43.0	3.4	4.7	1.0	1.0	1.0	4.7	Stable
PAB	2025	8.1	VerticalEnd	90	60.0	8.1	60.0	3.6	4.7	1.0	1.0	8.0	37.6	Stable
PAB	2025	8.1	HangingWall	90	60.0	61.0	43.0	12.6	1.5	1.0	0.5	8.0	6.0	Caved
PAB	2025	8.1	FootWall	90	60.0	61.0	43.0	12.6	2.7	1.0	0.8	8.0	17.3	Caved
PAB	2025	7.0	Back	90	60.0	7.0	83.0	3.2	4.7	1.0	1.0	1.0	4.7	Unstable
PAB	2025	7.0	VerticalEnd	90	60.0	7.0	60.0	3.1	4.7	1.0	1.0	8.0	37.6	Stable
PAB	2025	7.0	HangingWall	90	60.0	61.0	83.0	17.6	1.5	1.0	0.5	8.0	6.0	Caved
PAB	2025	7.0	FootWall	90	60.0	61.0	83.0	17.6	2.7	1.0	0.8	8.0	17.3	Caved
PAB	2050	9.5	Back	90	30.0	9.5	30.0	3.6	4.7	1.0	1.0	1.0	4.7	Stable
PAB	2050	9.5	VerticalEnd	90	30.0	9.5	30.0	3.6	4.7	1.0	1.0	8.0	37.6	Stable
PAB	2050	9.5	HangingWall	90	30.0	30.0	20.0	6.0	1.5	1.0	0.5	8.0	6.0	Unstable
PAB	2050	9.5	FootWall	90	30.0	30.0	20.0	6.0	2.7	1.0	0.8	8.0	17.3	Stable
PAB	2050	6.6	Back	90	30.0	6.6	20.0	2.5	4.7	1.0	1.0	1.0	4.7	Stable
PAB	2050	6.6	VerticalEnd	90	30.0	6.6	30.0	2.7	4.7	1.0	1.0	8.0	37.6	Stable
PAB	2050	6.6	HangingWall	90	30.0	30.0	20.0	6.0	2.7	1.0	0.5	8.0	10.8	Unstable

Table 11 continued

Mine Portal	Level	Orebody Thickness	Stope Surface	Surface Dip (°)	Height (m)	Span (m)	Length (m)	HR (m)	Q'	A	B	C	N'	Status
PAB	2050	6.6	FootWall	90	30.0	30.0	20.0	6.0	4.7	1.0	0.8	8.0	30.1	Stable
PAB	2050	5.6	Back	90	30.0	5.6	30.0	2.4	4.7	1.0	1.0	1.0	4.7	Stable
PAB	2050	5.6	VerticalEnd	90	30.0	5.6	30.0	2.4	4.7	1.0	1.0	8.0	37.6	Stable
PAB	2050	5.6	HangingWall	90	30.0	30.0	30.0	7.5	2.7	1.0	0.5	8.0	10.8	Unstable
PAB	2050	5.6	FootWall	90	30.0	30.0	30.0	7.5	4.7	1.0	0.8	8.0	30.1	Stable
PAB	2100	9.3	Back	90	30.0	9.3	43.0	3.8	4.7	1.0	1.0	1.0	4.7	Stable
PAB	2100	9.3	VerticalEnd	90	30.0	9.3	30.0	3.6	4.7	1.0	1.0	8.0	37.6	Stable
PAB	2100	9.3	HangingWall	90	30.0	30.0	43.0	8.8	2.7	1.0	0.5	8.0	10.8	Unstable
PAB	2100	9.3	FootWall	90	30.0	30.0	43.0	8.8	4.7	1.0	0.8	8.0	30.1	Unstable
PAB	2100	12.0	Back	90	30.0	12.0	35.0	4.5	4.7	1.0	1.0	1.0	4.7	Unstable
PAB	2100	12.0	VerticalEnd	90	30.0	12.0	30.0	4.3	4.7	1.0	1.0	8.0	37.6	Stable
PAB	2100	12.0	HangingWall	90	30.0	30.0	35.0	8.1	1.5	1.0	0.5	8.0	6.0	Caved
PAB	2100	12.0	FootWall	90	30.0	30.0	35.0	8.1	4.7	1.0	0.8	8.0	30.1	Unstable
PAB	2100	18.0	Back	90	30.0	18.0	60.0	6.9	71.3	1.0	1.0	1.0	71.3	Stable
PAB	2100	18.0	VerticalEnd	90	30.0	18.0	30.0	5.6	71.3	1.0	1.0	8.0	570.0	Stable
PAB	2100	18.0	HangingWall	90	30.0	30.5	60.0	10.1	8.1	1.0	0.5	8.0	32.5	Unstable
PAB	2100	18.0	FootWall	90	30.0	30.5	60.0	10.1	4.7	1.0	0.8	8.0	30.1	Unstable
PAB	2100	17.0	Back	90	30.0	17.0	60.0	6.6	71.3	1.0	1.0	1.0	71.3	Stable
PAB	2100	17.0	VerticalEnd	90	30.0	17.0	30.0	5.4	71.3	1.0	1.0	8.0	570.0	Stable
PAB	2100	17.0	HangingWall	90	30.0	31.0	60.0	10.2	8.0	1.0	0.5	8.0	32.0	Unstable
PAB	2100	17.0	FootWall	90	30.0	31.0	60.0	10.2	4.5	1.0	0.8	8.0	28.8	Unstable
PAB	2100	18.0	Back	90	30.0	18.0	60.0	6.9	71.2	1.0	1.0	1.0	71.2	Stable
PAB	2100	18.0	VerticalEnd	90	30.0	18.0	30.0	5.6	71.2	1.0	1.0	8.0	569.6	Stable
PAB	2100	18.0	HangingWall	90	30.0	33.0	60.0	10.6	7.9	1.0	0.5	8.0	31.6	Unstable
PAB	2100	18.0	FootWall	90	30.0	33.0	60.0	10.6	4.7	1.0	0.8	8.0	30.1	Stable
PAB	2125	17.0	Back	90	30.0	17.0	65.0	6.7	71.3	1.0	1.0	1.0	71.3	Stable
PAB	2125	17.0	VerticalEnd	90	30.0	17.0	30.0	5.4	71.3	0.8	1.0	8.0	437.7	Unstable
PAB	2125	17.0	HangingWall	90	30.0	30.5	65.0	10.4	6.0	1.0	0.8	6.8	32.6	Unstable
PAB	2125	17.0	FootWall	90	30.0	30.5	65.0	10.4	13.0	1.0	0.5	8.0	52.0	Stable
PAB	2125	6.6	Back	90	30.0	6.6	52.0	2.9	3.0	1.0	1.0	1.0	3.0	Stable
PAB	2125	6.6	VerticalEnd	90	30.0	6.6	30.0	2.7	3.0	1.0	1.0	8.0	24.0	Stable
PAB	2125	6.6	HangingWall	78	30.0	30.0	52.0	9.5	6.0	0.5	0.5	6.8	10.2	Stable
PAB	2125	6.6	FootWall	90	30.0	30.0	52.0	9.5	13.0	0.5	0.5	8.0	26.0	Stable
PAB	2150	8.1	Back	90	30.0	8.1	52.0	3.5	4.7	1.0	1.0	8.0	37.6	Stable
PAB	2150	8.1	VerticalEnd	90	30.0	8.1	30.0	3.2	4.7	1.0	1.0	8.0	37.6	Stable
PAB	2150	8.1	HangingWall	90	30.0	30.0	52.0	9.5	2.7	1.0	0.5	8.0	10.8	Caved
PAB	2150	8.1	FootWall	90	30.0	30.0	52.0	9.5	4.7	1.0	0.8	8.0	30.1	Unstable
PAB	2150	13.0	Back	90	30.0	13.0	50.0	5.2	4.7	1.0	1.0	1.0	4.7	Unstable
PAB	2150	13.0	VerticalEnd	90	30.0	13.0	30.0	4.5	8.3	1.0	1.0	8.0	66.4	Stable
PAB	2150	13.0	HangingWall	90	30.0	30.0	50.0	9.4	0.1	1.0	0.5	8.0	0.4	Caved
PAB	2150	13.0	FootWall	90	30.0	30.0	50.0	9.4	4.7	1.0	0.8	8.0	30.1	Unstable
PAB	2150	13.0	Back	90	30.0	13.0	50.0	5.2	4.7	1.0	1.0	1.0	4.7	Unstable
PAB	2150	13.0	VerticalEnd	90	30.0	13.0	30.0	4.5	8.3	1.0	1.0	8.0	66.4	Stable
PAB	2150	13.0	HangingWall	90	30.0	30.0	50.0	9.4	0.1	1.0	0.5	8.0	0.4	Caved

Table 11 continued

Mine Portal	Level	Orebody Thickness	Stope Surface	Surface Dip (°)	Height (m)	Span (m)	Length (m)	HR (m)	Q'	A	B	C	N'	Status
PAB	2150	13.0	FootWall	90	30.0	30.0	50.0	9.4	4.7	1.0	0.8	8.0	30.1	Unstable
PAB	2200	15.0	Back	90	107.0	15.0	60.0	6.0	2.7	1.0	1.0	8.0	21.6	Stable
PAB	2200	15.0	VerticalEnd	90	107.0	15.0	105.0	6.6	2.7	1.0	1.0	8.0	21.6	Stable
PAB	2200	15.0	HangingWall	90	107.0	107.0	60.0	19.2	8.3	1.0	0.5	8.0	33.2	Caved
PAB	2200	15.0	FootWall	90	107.0	107.0	60.0	19.2	4.7	1.0	0.8	8.0	30.1	Caved
PAB	2175	7.1	Back	90	30.0	7.1	65.0	3.2	2.7	1.0	1.0	1.0	2.7	Unstable
PAB	2175	7.1	VerticalEnd	90	30.0	7.1	30.0	2.9	2.7	1.0	1.0	8.0	21.6	Stable
PAB	2175	7.1	HangingWall	90	30.0	30.0	65.0	10.3	1.5	1.0	0.5	8.0	6.0	Unstable
PAB	2175	7.1	FootWall	90	30.0	30.0	65.0	10.3	4.7	1.0	0.8	8.0	30.1	Caved
PAB	2175	9.2	Back	90	30.0	9.2	55.0	3.9	8.3	1.0	1.0	1.0	8.3	Stable
PAB	2175	9.2	VerticalEnd	90	30.0	9.2	30.0	3.5	8.3	1.0	1.0	8.0	66.4	Stable
PAB	2175	9.2	HangingWall	90	30.0	30.0	55.0	9.7	2.7	1.0	0.5	8.0	10.8	Unstable
PAB	2175	9.2	FootWall	90	30.0	30.0	55.0	9.7	8.3	1.0	0.8	8.0	53.1	Unstable
PAB	2175	12.5	Back	90	30.0	12.5	40.0	4.8	8.3	1.0	1.0	1.0	8.3	Stable
PAB	2175	12.5	VerticalEnd	90	30.0	12.5	30.0	4.4	8.3	1.0	1.0	8.0	66.4	Stable
PAB	2175	12.5	HangingWall	90	30.0	30.0	40.0	8.6	2.7	1.0	0.5	8.0	10.8	Unstable
PAB	2175	12.5	FootWall	90	30.0	30.0	40.0	8.6	8.3	1.0	0.8	8.0	53.1	Stable
PAB	2175	12.2	Back	90	30.0	12.2	40.0	4.7	8.3	1.0	1.0	1.0	8.3	Stable
PAB	2175	12.2	VerticalEnd	90	30.0	12.2	30.0	4.3	8.3	1.0	1.0	8.0	66.4	Stable
PAB	2175	12.2	HangingWall	90	30.0	30.0	40.0	8.6	4.7	1.0	0.5	8.0	18.8	Unstable
PAB	2175	12.2	FootWall	90	30.0	30.0	40.0	8.6	2.7	1.0	0.8	8.0	17.3	Unstable
GAR	335L	10.2	FootWall	63	24.0	24.0	34.0	7.0	14.9	0.4	0.3	4.8	8.6	Caved
GAR	385L	6.0	FootWall	65	26.0	26.0	33.0	7.3	17.1	0.5	0.3	4.5	10.4	Unstable
GAR	285L	12.0	FootWall	81	27.0	27.0	38.0	7.9	25.4	0.6	0.3	2.7	12.3	Unstable
GAR	435L	6.0	FootWall	87	26.0	26.0	30.0	7.0	14.4	0.8	0.2	7.7	17.5	Unstable
GAR	235L	9.0	FootWall	79	25.0	25.0	34.0	7.2	29.8	1.0	0.3	6.7	55.8	Stable
GAR	435L	4.0	FootWall	72	26.0	26.0	22.0	6.0	17.0	0.6	0.3	6.2	16.4	Stable
GAR	435L	9.3	FootWall	56	31.0	31.0	27.0	7.2	36.6	0.3	0.3	4.6	12.8	Unstable
GAR	410L	6.0	FootWall	58	32.0	32.0	35.0	8.4	17.1	0.4	0.3	4.8	9.7	Caved
GAR	335L	12.7	FootWall	64	23.0	23.0	38.0	7.2	18.0	0.6	0.2	5.4	10.8	Unstable
GAR	335L	10.0	FootWall	80	25.0	25.0	30.0	6.8	13.4	0.5	0.3	3.1	5.7	Unstable
GAR	360L	6.7	FootWall	53	26.0	26.0	38.0	7.7	8.9	0.6	0.3	4.4	6.4	Caved
GAR	385L	7.7	FootWall	84	26.0	26.0	34.0	7.4	11.7	0.4	0.2	7.4	7.6	Unstable
GAR	485L	6.0	FootWall	61	27.0	27.0	35.0	7.6	18.5	0.3	0.3	5.1	7.4	Unstable
GAR	510L	5.0	FootWall	67	27.0	27.0	32.0	7.3	24.7	0.6	0.3	5.7	25.9	Stable
GAR	360L	15.0	FootWall	65	29.0	29.0	41.0	8.5	18.3	0.4	0.3	5.5	11.4	Unstable
GAR	235L	9.0	FootWall	82	25.0	25.0	40.0	7.7	21.4	0.8	0.2	3.9	13.3	Unstable
GAR	385L	9.0	FootWall	74	26.0	26.0	34.0	7.4	27.9	0.8	0.2	5.9	26.0	Stable
GAR	410L	8.0	FootWall	71	26.0	26.0	31.0	7.1	13.1	0.8	0.3	3.5	9.5	Unstable
GAR	385L	9.5	FootWall	53	30.0	30.0	30.0	7.5	8.7	0.8	0.2	4.4	7.4	Unstable
GAR	360L	9.0	FootWall	62	32.0	32.0	28.0	7.5	36.4	0.8	0.2	5.2	30.1	Stable
GAR	335L	10.2	HangingWall	63	24.0	24.0	34.0	7.0	5.4	0.7	0.3	4.8	5.4	Caved
GAR	385L	6.0	HangingWall	65	26.0	26.0	33.0	7.3	6.4	0.6	0.3	5.5	6.3	Caved
GAR	285L	12.0	HangingWall	81	27.0	27.0	38.0	7.9	3.8	0.6	0.3	7.1	4.5	Caved

Table 11 continued

Mine Portal	Level	Orebody Thickness	Stope Surface	Surface Dip (°)	Height (m)	Span (m)	Length (m)	HR (m)	Q'	A	B	C	N'	Status
GAR	435L	6.0	HangingWall	87	26.0	26.0	30.0	7.0	6.8	1.0	0.2	3.5	4.8	Caved
GAR	235L	9.0	HangingWall	79	25.0	25.0	34.0	7.2	6.5	0.8	0.3	3.3	4.9	Caved
GAR	435L	4.0	HangingWall	72	26.0	26.0	22.0	6.0	11.6	0.5	0.3	3.6	5.9	Unstable
GAR	435L	9.3	HangingWall	56	31.0	31.0	27.0	7.2	34.7	0.7	0.3	5.5	36.0	Stable
GAR	410L	6.0	HangingWall	58	32.0	32.0	35.0	8.4	34.1	0.5	0.3	5.0	23.9	Unstable
GAR	335L	12.7	HangingWall	64	23.0	23.0	38.0	7.2	9.8	0.6	0.2	3.5	4.1	Caved
GAR	335L	10.0	HangingWall	80	25.0	25.0	30.0	6.8	7.4	0.6	0.3	7.0	8.4	Unstable
GAR	360L	6.7	HangingWall	53	26.0	26.0	38.0	7.7	5.3	0.6	0.3	5.6	5.5	Caved
GAR	385L	7.7	HangingWall	84	26.0	26.0	34.0	7.4	17.8	0.4	0.2	4.7	7.0	Unstable
GAR	485L	6.0	HangingWall	61	27.0	27.0	35.0	7.6	10.1	0.5	0.3	5.0	7.3	Unstable
GAR	510L	5.0	HangingWall	67	27.0	27.0	32.0	7.3	22.8	0.4	0.3	4.4	11.1	Unstable
GAR	360L	15.0	HangingWall	65	29.0	29.0	41.0	8.5	7.7	0.5	0.3	4.5	4.7	Caved
GAR	235L	9.0	HangingWall	82	25.0	25.0	40.0	7.7	9.9	0.7	0.2	3.9	5.0	Caved
GAR	385L	9.0	HangingWall	74	26.0	26.0	34.0	7.4	8.7	0.3	0.2	6.4	3.5	Caved
GAR	410L	8.0	HangingWall	71	26.0	26.0	31.0	7.1	11.1	0.7	0.3	3.5	6.6	Unstable
GAR	385L	9.5	HangingWall	53	30.0	30.0	30.0	7.5	12.4	0.7	0.2	5.1	9.8	Unstable
GAR	360L	9.0	HangingWall	62	32.0	32.0	28.0	7.5	15.4	0.7	0.2	3.7	7.4	Unstable
YAL	283L	22.0	HangingWall	75	25.0	25.0	30.0	6.8	46.0	0.6	0.2	3.5	19.3	Unstable
YAL	283L	22.0	FootWall	75	25.0	25.0	30.0	6.8	32.0	0.6	0.2	3.5	13.4	Unstable
YAL	308L	28.0	HangingWall	66	25.0	25.0	30.0	6.8	44.0	0.8	0.2	4.4	31.0	Stable
YAL	308L	28.0	FootWall	66	25.0	25.0	30.0	6.8	25.0	0.8	0.2	4.4	17.6	Unstable
YAL	308L	30.0	HangingWall	79	25.0	25.0	20.0	5.6	38.0	1.0	0.3	3.1	35.3	Stable
YAL	308L	30.0	FootWall	79	25.0	25.0	20.0	5.6	25.6	1.0	0.3	3.1	23.8	Stable
YAL	383L	17.0	HangingWall	84	24.0	24.0	51.0	8.2	39.0	0.8	0.3	6.8	63.6	Stable
YAL	383L	17.0	FootWall	84	24.0	24.0	51.0	8.2	29.0	0.8	0.3	6.8	47.3	Unstable
YAL	408L	9.0	HangingWall	65	29.0	29.0	30.0	7.4	32.0	0.3	0.2	6.2	11.9	Unstable
YAL	408L	9.0	FootWall	65	29.0	29.0	30.0	7.4	18.0	0.3	0.2	6.2	6.7	Unstable
YAL	433L	22.0	HangingWall	72	25.0	25.0	51.0	8.4	14.9	0.6	0.2	7.4	13.2	Caved
YAL	433L	22.0	FootWall	72	25.0	25.0	51.0	8.4	21.1	0.6	0.2	7.4	18.7	Unstable
YAL	458L	13.0	HangingWall	71	28.0	28.0	55.0	9.3	27.3	0.8	0.2	3.9	17.0	Unstable
YAL	458L	13.0	FootWall	71	28.0	28.0	55.0	9.3	12.1	0.9	0.2	3.9	8.5	Caved
YAL	458L	6.0	HangingWall	63	26.0	26.0	41.5	8.0	12.0	0.6	0.2	4.7	6.8	Caved
YAL	458L	6.0	FootWall	63	26.0	26.0	41.5	8.0	3.4	0.6	0.2	4.7	1.9	Caved
YAL	458L	15.0	HangingWall	57	25.0	25.0	35.0	7.3	20.0	1.0	0.3	5.0	30.0	Stable
YAL	458L	15.0	FootWall	57	25.0	25.0	35.0	7.3	12.0	1.0	0.3	5.0	18.0	Unstable
YAL	483L	3.0	HangingWall	81	25.0	25.0	30.0	6.8	31.0	0.3	0.3	2.9	8.1	Unstable
YAL	483L	3.0	FootWall	81	25.0	25.0	30.0	6.8	9.0	0.3	0.3	2.9	2.3	Caved
YAL	483L	11.0	HangingWall	68	25.0	25.0	35.0	7.3	10.0	0.9	0.2	6.4	11.5	Unstable
YAL	483L	11.0	FootWall	68	25.0	25.0	35.0	7.3	7.0	0.9	0.2	6.4	8.1	Caved
YAL	508L	8.0	HangingWall	75	25.0	25.0	55.0	8.6	17.4	0.5	0.3	6.7	17.5	Unstable
YAL	508L	8.0	FootWall	75	25.0	25.0	55.0	8.6	19.7	0.6	0.3	6.7	23.8	Unstable
YAL	508L	4.0	HangingWall	60	25.0	25.0	31.0	6.9	25.0	0.2	0.2	7.2	7.2	Unstable
YAL	508L	4.0	FootWall	60	25.0	25.0	31.0	6.9	9.0	0.2	0.2	7.2	2.6	Caved
YAL	508L	5.0	HangingWall	79	26.0	26.0	30.0	7.0	20.0	0.5	0.2	3.1	6.2	Unstable

Table 11 continued

Mine Portal	Level	Orebody Thickness	Stope Surface	Surface Dip (°)	Height (m)	Span (m)	Length (m)	HR (m)	Q'	A	B	C	N'	Status
YAL	508L	5.0	FootWall	79	26.0	26.0	30.0	7.0	12.0	0.5	0.2	3.1	3.7	Caved
YAL	533L	5.0	HangingWall	84	25.0	25.0	35.0	7.3	14.0	0.3	0.3	7.2	9.1	Unstable
YAL	533L	5.0	FootWall	84	25.0	25.0	35.0	7.3	28.0	0.3	0.3	7.2	18.1	Unstable
YAL	283	18.0	HangingWall	88	15.0	15.0	55.0	5.9	12.0	0.6	0.3	7.3	15.8	Stable
YAL	283	18.0	FootWall	88	15.0	15.0	55.0	5.9	13.0	0.6	0.3	7.3	17.1	Stable
YAL	333	10.0	HangingWall	87	39.0	39.0	45.0	10.4	17.4	1.0	0.3	7.7	40.2	Unstable
YAL	333	10.0	FootWall	87	39.0	39.0	45.0	10.4	16.9	1.0	0.3	7.7	39.0	Unstable
YAL	358	12.0	HangingWall	53	24.5	24.5	35.0	7.2	16.0	0.5	0.2	7.4	11.8	Unstable
YAL	358	12.0	FootWall	53	24.5	24.5	35.0	7.2	19.0	0.5	0.2	7.4	14.1	Unstable
SAN	35L	6.2	HangingWall	72	60.0	6.9	60.0	3.1	0.9	1.0	0.2	6.1	1.2	Stable
SAN	35L	6.3	FootWall	70	60.0	7.0	58.0	3.1	1.5	1.0	0.2	8.0	2.4	Stable
SAN	35L	5.6	HangingWall	90	23.0	6.2	31.0	2.4	2.0	1.0	0.3	8.0	4.6	Stable
SAN	35L	5.5	FootWall	90	23.4	6.1	31.0	2.4	2.0	1.0	0.3	8.0	4.6	Stable
SAN	35L	8.7	FootWall	70	14.0	9.7	40.0	3.9	1.5	1.0	0.2	8.0	2.4	Stable
SAN	35L	9.0	HangingWall	90	13.9	10.0	32.2	2.9	2.0	1.0	0.3	8.0	4.6	Stable
SAN	35L	8.9	FootWall	90	14.0	9.9	32.2	2.9	2.9	1.0	0.3	8.0	6.7	Stable
SAN	30L	17.1	FootWall	79	23.0	19.0	15.0	4.2	20.0	1.0	0.2	8.0	35.2	Stable
SAN	30L	5.9	FootWall	85	30.0	6.6	30.0	2.7	8.8	1.0	0.2	7.5	13.2	Stable
SAN	30L	5.9	HangingWall	85	30.0	6.6	30.0	2.7	3.5	1.0	0.2	7.5	5.3	Stable
SAN	30L	5.2	Back	90	11.0	5.8	36.0	1.9	20.0	1.0	0.2	2.0	8.0	Stable
SAN	30L	10.2	FootWall	85	17.3	11.3	85.0	5.0	8.8	1.0	0.2	7.5	13.2	Stable
SAN	30L	15.1	HangingWall	85	20.3	16.8	41.0	4.6	3.5	1.0	0.2	7.5	5.3	Stable
SAN	30L	6.8	Back	90	20.8	7.6	48.0	3.3	15.0	1.0	0.2	2.0	6.0	Stable
SAN	30L	17.1	HangingWall	74	23.0	19.0	15.0	4.2	8.0	1.0	0.3	5.6	13.4	Stable
SAN	39L	24.2	HangingWall	66	14.4	26.9	15.0	4.8	1.6	1.0	0.3	5.6	2.7	Stable
SAN	39L	23.8	FootWall	66	14.4	26.4	15.0	4.8	3.0	1.0	0.3	3.8	3.4	Stable

References

Adoko, A.C., Yakubov, K. & Alipov, A. 2019. Mine stope performance assessment in unfavorable rock mass conditions using neural network-based classifiers. *YSRM2019 & REIF2019*. ISRM & The Japanese Society for Rock Mechanics., Okinawa, Japan.

Adoko AC, Vallejos J, Trueman R (2020) Stability assessment of underground mine stopes subjected to stress relaxation. Mining Technology: Transactions of the Institute of Mining and Metallurgy 129:30–39. https://doi.org/10.1080/25726668.2020.1721995

Capes, G.W. 2009. *Open stope hangingwall design based on general and detailed data collection in rock masses with unfavourable hangingwall conditions.* NR62618 Ph.D., The University of Saskatchewan (Canada).

Cepuritis, P.M., Villaescusa, E., Beck, D.A. & Varden, R. 2010. Back Analysis of Over-break In a Longhole Open Stope Operation Using Non-linear Elasto-Plastic Numerical Modelling. *44th U.S. Rock Mechanics Symposium and 5th U.S.-Canada Rock Mechanics Symposium*. American Rock Mechanics Association, Salt Lake City, Utah, 11.

Clark, L.M. 1998. *Minimizing dilution in open stope mining with a focus on stope design and narrow vein longhole blasting.* Master of Applied Science MSc Thesis, University of British Columbia.

Demuth H, Beale M (2002) Neural network toolbox for use with MATLAB, 4th edn. The MathWorks Inc, MA, USA

Diederichs MS, Kaiser PK (1996) Rock instability and risk analyses in open stope mine design. Can Geotech J 33:431–439. https://doi.org/10.1139/t96-064

Diederichs MS, Kaiser PK (1999) Tensile strength and abutment relaxation as failure control mechanisms in underground excavations. Int J Rock Mech Min Sci 36:69–96. https://doi.org/10.1016/S0148-9062(98)00179-X

Engelbrecht AP (2007) Computational Intelligence. Wiley, Chichester

García-Gonzalo E, Fernández-Muñiz Z, García Nieto P, Bernardo Sánchez A, Menéndez Fernández M (2016) Hard-Rock Stability Analysis for Span Design in Entry-Type Excavations with Learning Classifiers. Materials 9:531

Heidarzadeh S, Saeidi A, Rouleau A (2018) Evaluation of the effect of geometrical parameters on stope probability of failure in the open stoping method using numerical modeling. Int J Min Sci Technol. https://doi.org/10.1016/j.ijmst.2018.05.011

Henning JG, Mitri HS (2007) Numerical modelling of ore dilution in blasthole stoping. Int J Rock Mech Min Sci 44:692–703. https://doi.org/10.1016/j.ijrmms.2006.11.002

Mathews, K., Hoek, E., Wyllie, D. & Stewart, S. 1981. Prediction of stable excavation spans at depths below 1000m in hard rock mines. CANMET Report, DSS Serial No. OSQ80–00081.

Mawdesley C, Trueman R, Whiten WJ (2001) Extending the Mathews stability graph for open–stope design. Min Technol 110:27–39

Pakalnis, R. 2015. Empirical design methods in practice. *In*: Potvin, Y. (ed.) *Proceedings of the International Seminar on Design Methods in Underground Mining*. Australian Centre for Geomechanics, Perth, 37–56.

Pakalnis RT, Poulin R, Hadjigeorgiou J (1995) Quantifying the cost of dilution in underground mines. Min Eng 47:1136–1141

Potvin, Y. 1988. *Empirical open stope design in Canada.* PhD PhD Dissertation, The University of British Columbia.

Qi C, Fourie A, Du X, Tang X (2018a) Prediction of open stope hangingwall stability using random forests. Nat Hazards 92:1179–1197. https://doi.org/10.1007/s11069-018-3246-7

Qi C, Fourie A, Ma G, Tang X (2018b) A hybrid method for improved stability prediction in construction projects: A case study of stope hangingwall stability. Appl Soft Comput 71:649–658. https://doi.org/10.1016/j.asoc.2018.07.035

Qi C, Fourie A, Zhao X (2018c) Back-analysis method for stope displacements using gradient-boosted regression tree and firefly algorithm. J Comput Civ Eng 32:04018031

Rafiai H, Moosavi M (2012) An approximate ANN-based solution for convergence of lined circular tunnels in elasto-plastic rock masses with anisotropic stresses. Tunn Undergr Space Technol 27:52–59. https://doi.org/10.1016/j.tust.2011.06.008

Santos AEM, Amaral TKM, Mendonça GA, Silva, D.d.F.S.d. (2020) Open stope stability assessment through artificial intelligence. REM - International Engineering Journal 73:395–401

Stewart SBV, Forsyth WW (1995) The Mathews method for open stope design. CIM Bull 88:45–53

Stewart PC, Trueman R (2004) Quantifying the effect of stress relaxation on excavation stability. Min Technol 113:107–117. https://doi.org/10.1179/037178404225004986

Sunwoo C, Jung Y-B, Karanam UMR (2006) Stability assessment in wide underground mine openings by Mathews' stability graph method. Tunn Undergr Space Technol 21:246. https://doi.org/10.1016/j.tust.2005.12.024

Suorineni FT (2010) The stability graph after three decades in use: Experiences and the way forward. Int J Min Reclam Environ 24:307–339

Suorineni FT, Kaiser PK, Tannant DD (2001) Likelihood statistic for interpretation of the stability graph for open stope design. Int J Rock Mech Min Sci 38:735–744. https://doi.org/10.1016/S1365-1609(01)00033-8

Vallejos JA, Delonca A, Fuenzalida J, Burgos L (2016) Statistical analysis of the stability number adjustment factors and implications for underground mine design. Int J Rock Mech Min Sci 87:104–112. https://doi.org/10.1016/j.ijrmms.2016.06.001

Vallejos, J.A., Miranda, R., Burgos, L. & Perez, E. 2017. Development of New Design Tools for Open Stoping Underground Mines. *The 51st U.S. Rock Mechanics/Geomechanics Symposium*. American Rock Mechanics Association, San Francisco, California, USA, 8.

Wang J, Milne D, Pakalnis R (2002) Application of a neural network in the empirical design of underground excavation spans. Min Technol 111:73–81

Zhalel, M., Adoko, A.C. & Korigov, S. 2020. An Approach to Stope Stability Assessment in Open Stope Mining Environment. *54th U.S. Rock Mechanics/Geomechanics Symposium*. American Rock Mechanics Association, physical event cancelled, 6.